Highly charged ion based time-of-flight emission microscope

Alex V. Hamza,[a] Alan V. Barnes, Ed Magee, Mike Newman, Thomas Schenkel, Joseph W. McDonald, and Dieter H. Schneider
Lawrence Livermore National Laboratory, University of California, Livermore, California 94551

(Received 1 September 1998; accepted for publication 24 January 2000)

An emission microscope using highly charged ions as the excitation source has been designed, constructed, and operated. A novel ''acorn'' objective lens has been used to simultaneously image electron and secondary ion emission. A resistive anode-position sensitive detector is used to determine the $x-y$ position and time of arrival of the secondary events at the microscope image plane. Contrast in the image can be based on the intensity of the electron emission and/or the presence of particular secondary ions. Spatial resolution of better than 1 μm and mass resolution $m/\Delta m$ of better than 400 were demonstrated. Background rejection from uncorrelated events of greater than an order of magnitude is also achieved. *© 2000 American Institute of Physics.* [S0034-6748(00)03105-1]

I. INTRODUCTION

The past decade has seen the increasingly sophisticated demands made of the semiconductor industry for highly sensitive materials characterization at high spatial resolution drive instrument development. An impressive array of instruments is available to achieve very high-resolution lateral imaging of materials (transmission electron microscopy, scanning electron microscopy, scanning tunneling microscopy, etc.). There is an equally impressive array of instruments and techniques available with which to determine material composition (secondary ion mass spectroscopy, Auger electron spectroscopy, photoelectron spectroscopy, etc.). We report here on a new emission microscopy technique with the potential to offer ***both*** high spatial resolution and very sensitive compositional analysis, *simultaneously*. This prototype instrument is designed and built to demonstrate the concepts necessary to construct a higher resolution instrument.

The common technology shared by emission microscopes, which are a special class of electron microscopes, is the accelerating and imaging of low energy electrons and/or other charged particle emitted or reflected from a planar surface. Emission microscopy has a more than 100 year history. For a review the reader is referred to Ref. 1. The present instrument is a combination of two emission microscopes developed in the 1960s. The first was the Ar^+ ion beam induced electron emission microscope[2] where the kinetic emission of electrons forms an image. The second was the secondary ion emission microscope[3] where an ion beam is used to sputter secondary ions, which are imaged. Both instruments eventually became commercially available through Balzers and CAMECA. The present instrument represents an advance in that *both* electrons and secondary ions are imaged and the mass of the secondary ions is determined by time of flight so that all the secondary ions are detected simultaneously. Thus, a large variety of contrast imaging modes is available.

The emission microscope described here uses highly charged ions (HCIs) as the excitation source. The highly charged ion source brings four crucial advantages, a large secondary electron yield, high secondary ion yields, high ionization probability of the secondary emission, and high molecular ion yields.

Highly charged ions bring considerable potential energy (the sum of the ionization potentials of the highly charged ion) to surfaces and it is all released in the first few femtoseconds of surface interaction resulting in a highly localized energy deposition.[4] In contrast is the case of singly charged ion induced secondary ion mass spectroscopy (SIMS) where most of the energy transferred to the surface comes from the kinetic energy of the projectile ion. The kinetic transfer is a multistep, relatively low cross section process and thus is not localized at the surface but is distributed across a compara-

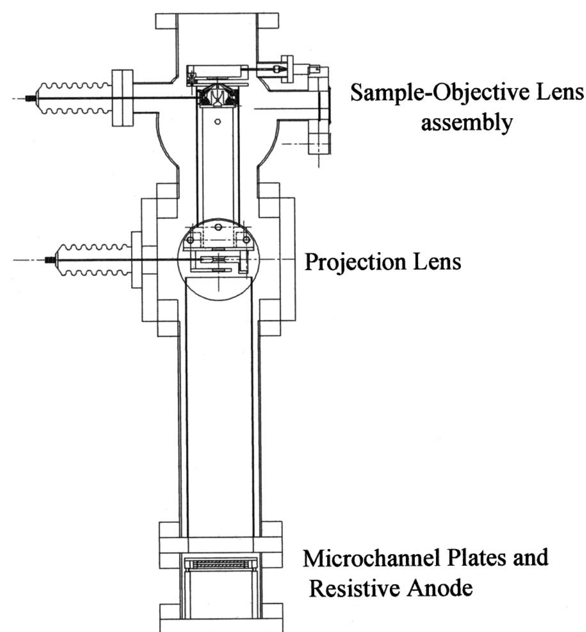

FIG. 1. Schematic of the highly charged ion based time-of-flight emission microscope.

[a]Electronic mail: hamza1@llnl.gov

 © 2000 American Institute of Physics

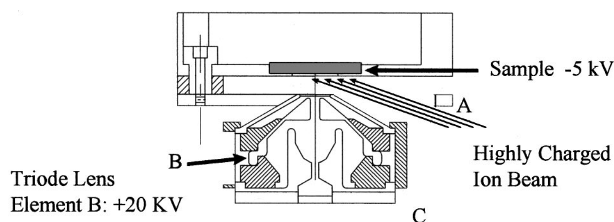

FIG. 2. Schematic of the ''acorn'' objective lens. Elements (A) and (C) are at ground potential. Element (B) can be biased to +40 kV. The sample is mechanically attached to the lens and can be biased to +/−5 kV.

tively deep collision cascade. The localized energy deposition from a HCI impact results in very high (100's of electrons per primary ion) electron yields[5,6] and (greater than one) secondary ion yields.[7] The ratio of the secondary ion yield to the secondary neutral yield gives ionization probabilities of 10% for HCI excitation.[8] The high electron yield enables the potential to achieve very high spatial resolution. Present photoelectron emission microscopes can achieve less than 10 nm resolution imaging single electron events.[9] The high secondary ion yield, particularly the high secondary molecular ion yield, and the high ionization probability that HCI excitation produces offer the potential of providing highly sensitive composition information at a high spatial resolution.

II. EXPERIMENT

A low emittance beam ($<1\ \pi$ mm mrad) of highly charged ions was extracted from the electron beam ion trap (EBIT) at Lawrence Livermore National Laboratory.[10] A 90° bending magnet in the beamline between the EBIT and the microscope chamber (base pressure 3×10^{-7} Pa) is used to select the mass-to-charge ratio of the incident ion beam. A schematic of the microscope is shown in Fig. 1. The sample

FIG. 3. Highly charged ion based emission microscope image of (a) 10 μm copper lines surrounded by SiO_2 on 30 μm centers. (b) Light microscope image of a similar region of the wafer. (c) A highly charged ion microscope image of 800 nm copper lines on 2400 nm centers. The magnification of all images is ~500×. See the text for a description of the different contrast modes.

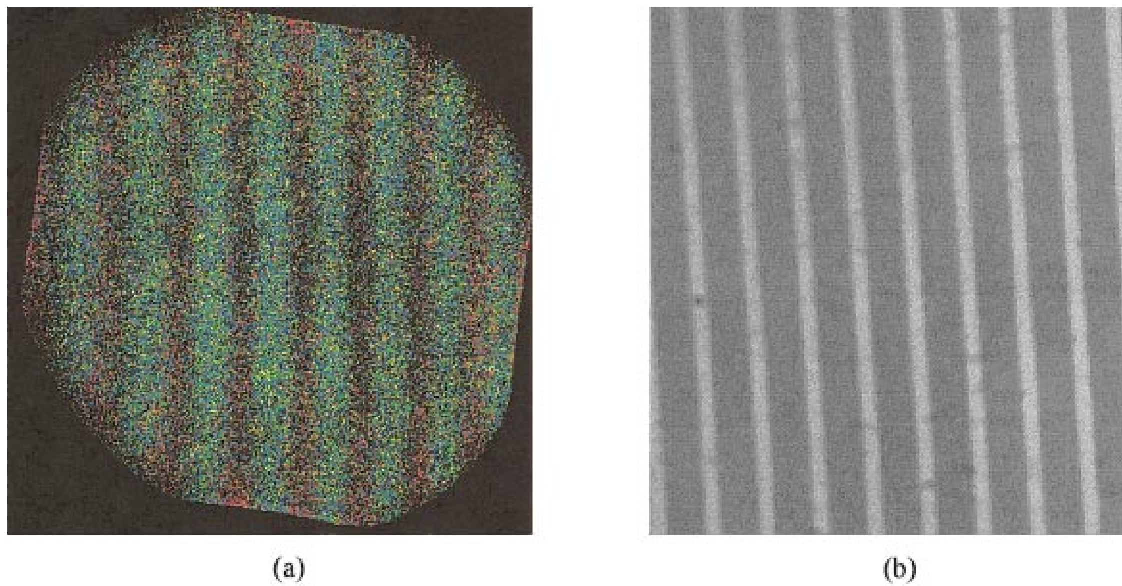

FIG. 4. Positive ion contrast in highly charged ion microscopy. (a) Image of 5 μm copper lines on 15 μm centers. (b) Light microscope image of a similar area. The magnification is approximately 500× in both images. The contrast in (a) is based on the time of flight of the secondary ion. Short flight times are represented by blue and green and long flight times by red.

plane is 5 mm from the objective lens. A projection lens is 200 mm from the sample plane and the 40 mm multichannel plate detector is 460 mm from the sample plane. The 3 mm HCI beam spot illuminates the entire 1 mm field of view. For all the data collected in this article a Xe^{44+} beam was used. The flux of ions to the surface was limited by the 4000 ions/s rate the data acquisition system could handle.

SIMION 3D Ver. 6.0 software[11] was used to design the objective lens.[12] The constraints for this lens, which are different from other emission microscope objective lenses, are that both secondary electrons and secondary ions are to be imaged and a highly charged ion beam has to pass the objective lens and impinge upon the sample. These two are opposing constraints, since a high accelerating field at the sample is desired in order to collect secondary particles with minimal aberrations and a very high accelerating field will deflect the primary HCI beam. The resulting ''acorn'' design is shown in Fig. 2. The top (A) and rear (C) elements are held at ground potential like they are in many photoelectron emission microscope designs.[9] The top element has six evenly spaced slots in it; one of these is aligned so that the highly charged ion beam can pass through element (A) to impinge on the sample in the field of view. The second element (B), which reaches inside the top element also to within 5 mm of the sample plane, is the focusing element, which can be biased from 0 to +/−40 kV. The novel shape of elements (B) and (C) produces a relatively uniform electric field gradient in the lens that is capable of imaging both secondary electrons and ions. The microscope operated with just the objective lens has a magnification of ~40×.

Microchannel plates with a resistive-anode readout (Gallileo Electro Optics Corporation) was used to record the po-

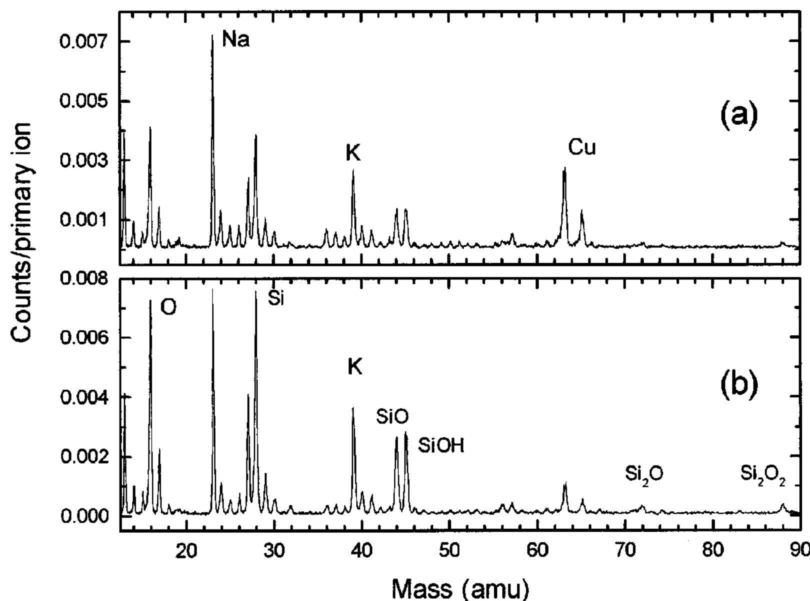

FIG. 5. Time-of-flight spectrum (a) from the copper lines and (b) from the SiO_2 region.

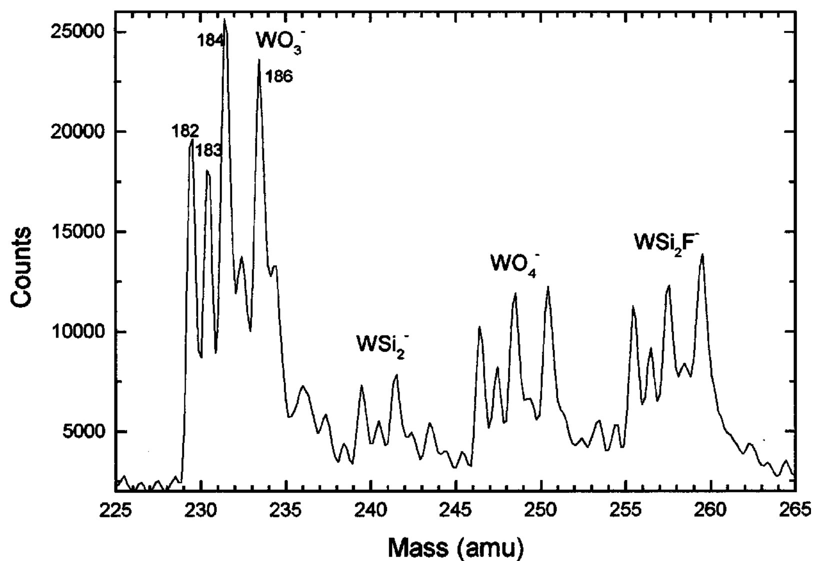

FIG. 6. Time-of-flight spectrum demonstrating greater than 1 amu mass separation out to mass 260 from a tungsten/silicon dioxide wafer sample.

sition of the electrons and ions arriving at the microscope image plane. The electronics recorded data records for each event containing the pulse heights from the detector for the start (electron secondaries) and stop (ion secondaries) as well as the time interval between the start and stop. Images can be constructed by a variety of postprocessing procedures. For example, images may be constructed by displaying the pulse height of the start (electron) pulse as a function of the $x-y$ position with or without requiring certain secondary ion filters. Images can also be displayed using the $x-y$ position from the start pulse and a color for the time of arrival of the stop. In addition time-of-flight spectra from all the events or from events in a particular region can be displayed.

III. RESULTS AND DISCUSSION

Figures 3 and 4 depict images collected from silicon wafers that have pads of copper lines (sample supplied by H. Li, On-Trak Technologies, Inc.). The widths of the copper lines ranged from 500 nm to 150 μm. The sample layout is as follows. SiO_2 films with a thickness of 800 nm were deposited onto a silicon substrate by plasma enhanced chemical vapor deposition. The SiO_2 was etched to form trenches after a single mask photolithographic process. After etching the wafer was coated with a 25 nm thick Ta diffusion barrier layer by physical vapor deposition. This was followed by physical vapor deposition of a 50 nm thick copper ''seed'' layer. Then a copper layer with an excess thickness of 1 μm was electroplated onto the wafer, filling the trenches and blanketing the whole wafer surface. The excess copper and tantalum were removed by chemical mechanical polishing to expose the SiO_2 and to form the Cu lines and pads. After polishing the wafers are cleaned by a double-sided scrubber. The cleaning solution during scrubbing was de-ionized water. Figure 3(a) is an image of 10 μm copper lines on 30 μm centers. The color contrast in the image indicates the number of the electron emission events, the red being the highest number of events and purple the lowest number of events. The copper areas emit more electrons per highly charged ion impact than the silicon dioxide. The electron contrast results from the different emission yields,[13] which is particularly significant at high charge states. The magnification in this image is $\sim$500 $\times$, which is achieved with the electrostatic

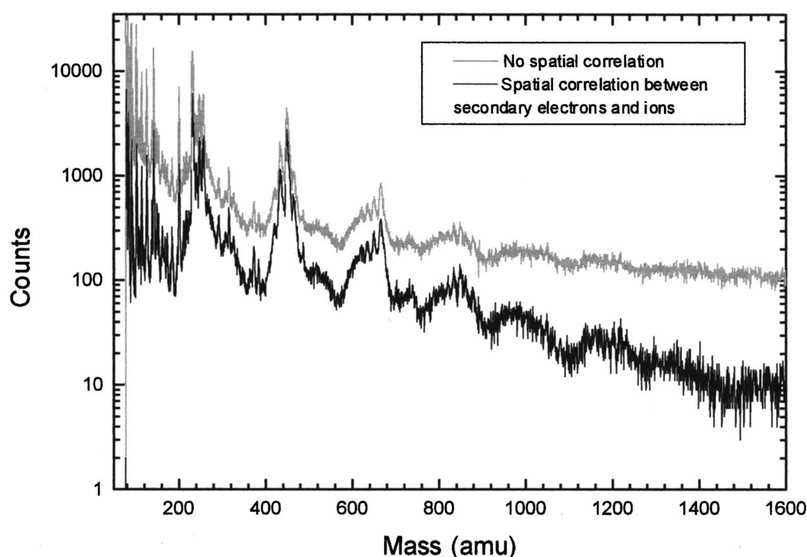

FIG. 7. Comparison of the time-of-flight spectrum for all events from the wafer (gray line) and the time-of-flight spectrum for events where the secondary ion arrival is spatially correlated with the electron pulse (black line).

projection lens. Figure 3(b) is a light microscope image of the same copper lines for comparison at approximately the same magnification. Figure 3(c) is an image of 800 nm copper lines on 2400 nm centers. The image is collected also using electron pulse height contrast, and displays only a narrow distribution of pulse heights. The magnification in this image is also ~500 ×. This image represents the best lateral resolution we have achieved to date.

Figure 4(a) is a positive ion image from an area of the wafer with 5 μm lines on 15 μm centers. The start pulse in the positive secondary ion case is the proton pulse. The color contrast in this image corresponds to the type of secondary ion observed measured by time of flight. The red corresponds to long time, hence heavier ions such as Cu^+; the green corresponds to shorter flight times such as SiO^+. Figure 4(b) is a light microscope image of the same region with the same magnification (500×). The images displayed in Figs. 3 and 4 collected with the highly charged ion microscope are composed of from between 1 and 2 million ion events and were collected in 5–20 min. With a sputter yield of less than 100 secondary particles per incident primary ion,[8] less than 10^{-6} monolayer is removed collecting an image.

The image in Fig. 4(a) reveals two significantly different material regions. There are copper lines and SiO_2 regions. Postcollection analysis of the image can provide a spatially resolved analysis of the composition by selecting events from copper or SiO_2 regions. Figure 5(a) shows the time-of-flight spectrum from three of the copper lines (5 μm× ~75 μm each), while Fig. 5(b) is the spectrum of a SiO_2 region (three regions, 10 μm×~75 μm each). Figure 5(b) shows the characteristic mass peaks associated with SiO_2, Si^+, SiO^+, and $SiOH^+$. The plot in Fig. 5(a) shows an enhanced Cu^+ feature and reduced Si^+ and SiO^+ features. Because this sample has been covered with copper and subsequently polished, copper and SiO_2 are everywhere on the sample. It is a testament to the polishing and cleaning capabilities that ion contrast is still possible. The negative ion time-of-flight spectra were dominated by carbon cluster ions and no negative ion contrast was observed from the copper/silicon dioxide wafer.

The time-of-flight spectrum obtained with this initial test of the microscope was also respectable. Figure 6 shows a time-of-flight spectrum from the microscope taken with an Ortec picosecond time analyzer while accumulating an image from a tungsten/silicon dioxide test wafer. The chemical vapor deposited tungsten/SiO_2 test silicon wafer was not polished and hence showed good ion contrast in the both positive and negative time-of-flight spectrum. We can clearly resolve the isotopes of tungsten (182, 26%; 183, 14%; 184, 31%; 186, 28%) in the tungsten oxide negative secondary ion spectrum at masses out to 260 amu.

Substantial background suppression can be achieved by eliminating uncorrelated stop events from the time-of-flight spectrum. Selected events are required to have all their ions in the same location. This allows secondaries from several events in the spectrometer at the same time with no confusion about which secondary goes with which event. Figure 7 illustrates the rejection of a ''pileup'' of background by only selecting events whose secondary ions arrive in the same location as the secondary electrons. Figure 7 shows an increase in the signal-to-noise ratio of nearly an order of magnitude for the secondary ion mass spectrum. Assuming reasonable detector resolutions, this procedure can reduce background from pileup by many orders of magnitude. In principle the primary beam intensity could be increased by this amount, enabling images of a 10 μ region with 100 nm resolution to be acquired in a few seconds. In practice, the bandwidth limitations of the position sensing devices will allow only a three order of magnitude improvement in collection times, but the increased sensitivity due to reduced pileup background will still be a benefit.

A highly charged ion based time-of-flight emission microscope has been designed, constructed, and demonstrated. The prototype instrument serves as a test bed for future development. Highly charged ion based SIMS has the potential to improve the surface sensitivity of static SIMS measurements because of the higher ionization probability than in measurements using singly charged ions.[8] This new instrument (described above and future improvements of it) ***combines*** high surface sensitivity (10^{10} atoms/cm^2)[8] with high spatial resolution (800 nm demonstrated with highly charged ions in this article and 8 nm demonstrated with photoelectron emission microscopy[9]) and chemical structure information (due to the high molecular ion yields).[14] In addition the high secondary ion yield affords coincidence counting in the SIMS measurement, which can be used to enhance determination of the chemical and topological structure.[15,16]

ACKNOWLEDGMENT

This work was performed under the auspices of the U.S. Department of Energy at Lawrence Livermore National Laboratory under Contract No. W-7405-ENG-48.

[1] O. H. Griffith and W. Engel, Ultramicroscopy **36**, 1 (1991).
[2] H. Düker, Z. Metallkd. **51**, 314 (1960).
[3] R. Castiang and G. Slodzian, *Proceedings of the European Regional Conference on Electron Microscopy* (Nederlanse Vereniging voor Electron Microscopic, Delft, 1960), Vol. 1, p. 169.
[4] T. Schenkel, M. A. Briere, H. Schmidt-Böcking, K. Bethge, and D. H. Schneider, Phys. Rev. Lett. **78**, 2481 (1997).
[5] J. McDonald, D. Schneider, M. Clark, and D. DeWitt, Phys. Rev. Lett. **46**, 2297 (1992).
[6] F. Aumayr, H. Kurz, D. Schneider, M. Briere, J. W. McDonald, C. E. Cunningham, and H. P. Winter, Phys. Rev. Lett. **71**, 1943 (1993).
[7] T. Schenkel, A. V. Barnes, M. A. Briere, A. Hamza, A. Schach von Wittenau, and D. H. Schneider, Nucl. Instrum. Methods Phys. Res. B **125**, 153 (1997).
[8] T. Schenkel, A. V. Barnes, A. V. Hamza, D. H. Schneider, J. C. Banks, and B. L. Doyle, Phys. Rev. Lett. **80**, 4325 (1998).
[9] G. F. Rempfer and O. H. Griffith, Ultramicroscopy **47**, 35 (1992).
[10] D. Schneider, M. W. Clark, B. M. Penetrante, J. McDonald, D. DeWitt, and J. N. Bardsley, Phys. Rev. A **44**, 3119 (1991).
[11] D. A. Dahl, 43rd ASMS Conference on Mass Spectrometry and Allied Topics, Atlanta, GA, 21–26 May 1995, p. 717.
[12] A. V. Barnes (unpublished).
[13] A. V. Hamza, T. Niedermayr, T. Schenkel, M. Newman, G. Machicoane, J. McDonald, and A. V. Barnes (unpublished).
[14] A. V. Hamza, T. Schenkel, and A. V. Barnes, Eur. Phys. J. D **6**, 83 (1999).
[15] A. V. Hamza, A. V. Barnes, T. Schenkel, and D. H. Schneider, J. Vac. Sci. Technol. A **17**, 303 (1999).
[16] M. A. Park, K. A. Gibson, L. Quinones, and E. A. Schweikert, Science **248**, 988 (1990).